



## THREE-DIMENSIONAL PLATE AND CONTACT/FRICTION ELEMENTS FOR LAMINATED COMPOSITE JOINTS

E. J. Barbero,<sup>†</sup> R. Luciano<sup>‡</sup> and E. Sacco<sup>‡</sup>

<sup>†</sup>Department of Mechanical and Aerospace Engineering, West Virginia University Morgantown, WV 26506, U.S.A.

<sup>‡</sup>Department of Industrial Engineering, University of Cassino, Italy

(Received 7 August 1993)

**Abstract**—A contact/friction isoparametric finite element for the analysis of connections between laminated composite plates is presented. The element is compatible with a three-dimensional plate element based on layer-wise constant shear theory. The contact/friction element is based on a simple regularization of the unilateral contact with an orthotropic Coulomb friction problem. Two different friction coefficients in orthogonal directions and a constitutive law to model slip in any direction are used to account for the orthotropic surface texture of fiber-reinforced materials. The contact and friction constitutive law is distributed over the entire surface in contact/friction. The integration scheme is chosen to accurately account for the partial contact and slip inside the element, thus avoiding unnecessary mesh refinement. Unlike nodal gap elements, the proposed element applies the contact and friction constitutive laws uniformly over the contact/friction surface regardless of mesh refinement or element distortion. The irreversibility of the process leads to unsymmetric secant stiffness matrix. However, an iterative procedure working on symmetric matrices is proposed. Finally, numerical results are presented.

### 1. INTRODUCTION

Composite materials are very good candidates to replace and complement conventional materials like steel, aluminum or concrete, because of light weight, corrosion resistance, electromagnetic transparency, etc. Previous studies have demonstrated that connections performance is one of the more important limiting factors for the application of composites. Bolted connections are preferred because they facilitate construction, they can be disassembled, facilitate rehabilitation of damaged structures, and they are considered safer than bonded connections for long life cycles. Experimental evidence [1] suggests the possibility that friction plays an important role in the bolted and the bonded-bolted connections strength. The amount of the torque is found [1] to influence the ultimate strength of both bolted and bonded-bolted connections which may indicate that slip occurs at different levels of load. Furthermore, experimental evidence indicates that the rupture in composite material structures occurs suddenly with brittle behavior, hence in a structure subjected to impact or earthquake loads, a large amount of energy can be absorbed by the friction developed in the connections. Furthermore, stresses are not transferred from bolt to hole until slip occurs. Hence, the friction occurring between jointed plates improves the efficiency of the connections. However, friction effects are often neglected in the analysis of fastened connections [2], because of the difficulty involved in its treatment. On the contrary, it is our belief that it is

necessary to overcome these difficulties and to properly account for the friction in bolted connections. Unilateral contact must be considered to properly take into account the partial contact between jointed plates, because some separation in the region between the jointed parts always occurs due to the deformation under load and bolt torque. In order to develop a realistic analysis of bolted connections it is then necessary to consider appropriate plate and contact/friction models. Both a three-dimensional (3D) plate element and a compatible interface element are introduced next.

Many of the analysis tools for laminated composite plates are based on the kinematic assumptions introduced by Reissner and Mindlin, which constitute the basis for the first-order shear deformations theory (FSDT) [3]. FSDT produces excellent results for global response (e.g., deflections) but the accuracy of the stress distribution is not adequate for the analysis of bolted connections and other unilateral contact and friction problems of thick laminated composites structures. Higher order theories have been proposed in an attempt to improve the prediction of stresses, but only limited success has been possible with equivalent single-layer theories. All of the equivalent single layer theories have a common characteristic: the assumed distribution of the displacements through the thickness has continuous derivatives with respect to the thickness coordinate. This implies that the out-of-plane shear strains are continuous across the material interfaces. As a result of the different material properties, the out-of-plane stress

components are discontinuous at the interfaces between layers, thus violating the equilibrium conditions.

To overcome the limitations of the single-layer theories and to obtain a good evaluation of the stresses, a new class of theories has emerged which is based on a distribution of the displacement through the thickness that is continuous but with discontinuous derivatives at the interfaces between layers. If the distribution of displacement is linear in the thickness coordinate for each layer, the kinematics leads to layer-wise constant shear (LCS) theories, which were developed by several authors [4–12]. For the modeling of joints, a disadvantage of 2D plate theories is the need to use multi-point constraints to joint the middle surface of the two components of the joint. This problem could be avoided by using 3D continuum elements, but plate elements are universally used to analyze laminated composite plates because of the cost of 3D analysis. The main disadvantage of conventional continuum 3D elements, when used to analyze each layer of a composite plate individually, is the large number of degrees of freedom (DOF) involved, since the aspect ratio of the element limits the surface dimensions of the elements to no more than one order of magnitude larger than the thickness of a layer.

A new element was developed by Barbero [12, 13] using the idea of the 3D shell element of Ahmad *et al.* [14] and using the kinematic constraints of LCS theories. With the use of this special 3D plate element, it is possible to analyze laminated composite plates overcoming the difficulties of both the LCS 2D elements and the continuum 3D elements but retain-

ing the precise stress calculation. It is important to note that, because in this element the position of the middle surface is irrelevant, it is possible to model joint problems (e.g., lap joints) without using multi-point constraints, which are needed in conjunction with regular plate elements to link the middle surfaces of the connected plates.

The unilateral contact with Coulomb friction constitutive relationships between the contact stress and the relative displacement vectors are governed by nondifferentiable, nonconvex and noncoercive functionals. In particular the nondifferentiability of these governing functionals is due, for the unilateral problem, to the requirement of absolute rigid contact of the two surfaces, and, for the friction problem, to the sliding or full adhesion of the contact surface [15, 16]. Therefore, the contact/friction problem is complex both from a theoretical and computational point of view. On the other hand, experiments show that this description of the contact is unrealistic. In fact, it has been found that when surfaces are in contact they may deform somewhat under normal pressure because of the irregularities and asperities of the surfaces. Moreover, tests on the friction phenomena emphasize that no such line of separation of sliding and full adhesion exists. Researchers working on tribology proposed [17] an exponential equation to describe the normal behavior of the interface and a polynomial equation for the friction.

These facts suggest using approximate regularized functionals for the unilateral and friction contact constitutive relationships. Regularized constitutive equations have been proposed [18, 19] for the static and dynamic 2D analysis of monumental structures

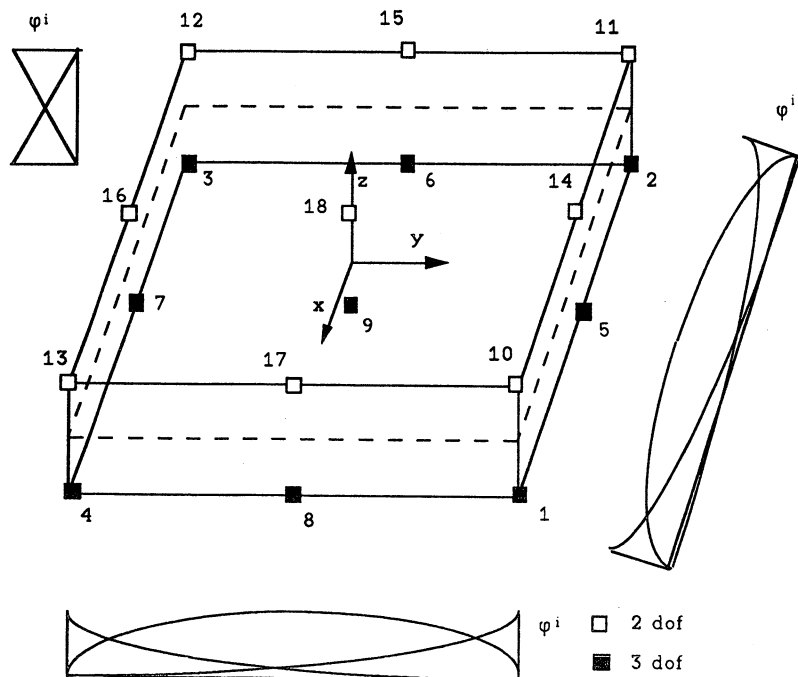


Fig. 1. Three-dimensional plate element.

made by superimposed blocks. An extension of the regularized constitutive equations is made herein for 3D problem with orthotropic friction.

Once the constitutive equations for the contact/friction problem are introduced, the isoparametric 3D finite interface element can be derived. Several interface elements can be found in the literature. Most of the joint elements implement connections directly between the nodes defined by the finite element mesh, by means of 1D springs. A 2D displacement based interface element was presented by Goodman *et al.* [20] to analyze the behavior of jointed rocks. This element, to the best of the authors' knowledge, was the first full interface element, in the sense that it accounts for springs uniformly distributed along one line which connects two surfaces in contact. The analysis was limited to 2D plane strain or plane stress problems and the interface behavior was essentially linear. Then, displacement-based interface elements for 3D nonlinear analysis has been proposed, for instance in [21, 22].

The interface element proposed herein is based on an isoparametric formulation, is consistent with the standard 3D continuum elements and with the new 3D plate element, it can account for a trivial or not trivial initial gap distance between the two surfaces in connection, and it can consider two different friction coefficients in orthogonal directions. Both the 3D plate and the 3D interface finite elements are based on the displacement formulation. This is convenient for its simplicity and ease of implementation in commercial finite element packages, which generally use spring connections between nodes to simulate the friction/contact behavior of the interface. Nodal springs induce a non-uniform regularization in the space of the unilateral Coulomb law when the mesh is not uniform. Therefore, both mesh refinement and distorted elements create a model with non-uniform constitutive interface law. It will be shown that the proposed plate and interface elements provide a more rational formulation of the problem at hand, using uniformly distributed regularization of the contact and friction applied directly on the context displacement-based 3D plate elements.

## 2. PLATE ELEMENT

Consider a laminated plate composed of  $n$  orthotropic laminae, each arbitrarily oriented with respect to the global coordinate system ( $x$  and  $y$  in the middle plane of the plate and  $z$  in the thickness direction). Each layer of the plate is discretized by 3D plate elements. The displacement  $\mathbf{u} = \{u, v, w\}^T$  inside an element is given by

$$\mathbf{u} = \mathbf{N}\mathbf{U}, \quad (1)$$

where  $\mathbf{U}$  is the vector of the nodal displacements  $\mathbf{d}^i = \{u^i, v^i, w^i\}^T$  with  $i = 1, \dots, m$ ,  $m$  is the number of the nodes in the element, and  $\mathbf{N}$  is the matrix of the

interpolation functions  $\phi^i$ . The order of interpolation  $\phi^i$  along the two directions on the surface of the element (Fig. 1) can be chosen independently of the order through the thickness. Linear or quadratic interpolation of the displacements ( $u, v$ ) and the geometry ( $x, y$ ) are commonly used. The order of approximation in the thickness direction corresponds to different kinematical assumptions in LCS theories. In this paper, and consistently with the findings of Barbero [11], a linear variation is used. The quadratic element has 18 nodes. Nodes 1–9 have three DOF ( $u, v$  and  $w$ ), nodes 10–18 have two DOF ( $u$  and  $v$ ) as shown in Fig. 1. The variables  $u$  and  $v$  correspond to the in-plane displacements at the interfaces between elements (layers). The quadratic element has a total of 45 DOF.

The transverse deflection is constant through the thickness by the incompressibility assumption. Therefore, the DOF of two nodes aligned through the thickness of an element can be reduced to a single DOF (for example,  $w$  in the bottom filled squares in Fig. 1). Then, at the element level the stiffness matrix is rearranged so that the DOF corresponding to the displacements  $u$  and  $v$  on the surface of the plate for all nodes (e.g., 18 nodes) are grouped first. The remaining DOF corresponding to  $w$ -displacements are assigned to a new set of nodes (e.g. nine nodes) called  $w$ -master nodes. The location of the  $w$ -master nodes through the thickness of the laminate does not affect the results. The resulting element has 18 nodes with two DOF ( $u$  and  $v$ ) and nine nodes with one DOF ( $w$ ) per node.

If more than one layer is used to model the laminate, another condensation must be done for each vertical because the  $w$ -displacements are identical. A three-layer laminate modeled with three elements is shown in Fig. 2. Since the transverse deflection  $w$  is constant through the thickness, a single global node connects all the local  $w$ -nodes that lie on a line perpendicular to the middle surface.

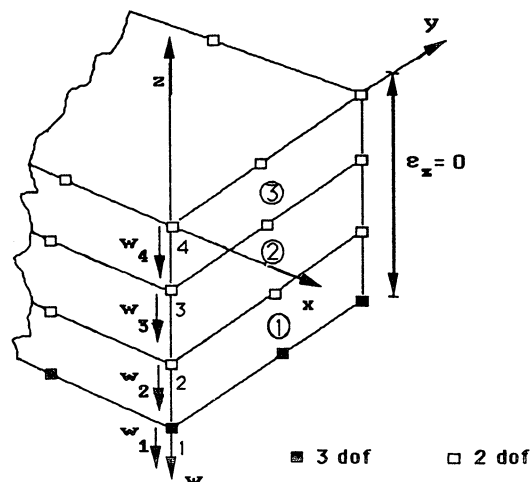


Fig. 2. Schematic representation of the degrees of freedom used in a three-layer model using 3D plate elements.

Then, only one  $w$ -master node (e.g., the one at the bottom of the laminate, solid squares in Fig. 2) must be retained. This condensation has been achieved by assigning the same global node number to all the  $w$ -master nodes through the thickness of the laminate at a given surface location  $(x, y)$ . This technique eliminates the need for complex book-keeping to identify individual sets of elements stacked to form a laminate. Furthermore, the present formulation eliminates the need for elements with large number of DOF per node, typical of 2D finite element implementations of LCS theories, which would result if the assembly through the thickness were performed *a priori*. This feature is particularly useful for implementation in commercial finite element programs. The strain vector is:

$$\boldsymbol{\epsilon} = \begin{Bmatrix} \epsilon_x \\ \epsilon_y \\ \gamma_{yz} \\ \gamma_{xz} \\ \gamma_{xy} \end{Bmatrix} = \begin{Bmatrix} u_{,x} \\ v_{,y} \\ w_{,y} + v_{,z} \\ w_{,x} + u_{,z} \\ u_{,y} + v_{,x} \end{Bmatrix} \quad (2)$$

with the strain in the direction  $z$  neglected to be consistent with the incompressibility of the normals implicit in the plate LCS theory. The layer-wise constant shear constraint is satisfied by virtue of the linearity through the thickness of the displacements  $u$  and  $v$  in eqn (1) resulting from the choice of interpolation functions  $\varphi^i$  that are linear through the thickness (Fig. 1).

The constitutive equations for the  $k$ th layer (or element) of an orthotropic material, oriented arbitrarily with respect to the elemental coordinate system, are obtained in a similar way to that of a monoclinic material [23]. To overcome the locking effect that a vanishing transverse strain would have, the element constitutive matrix is a combination of the 2D rotated reduced stiffness terms  $Q_{ij}$  [23] and 3D terms  $C_{ij}$  [24]. In this way we obtain

$$\bar{\mathbf{D}}^k = \begin{bmatrix} Q_{11}^k & Q_{12}^k & 0 & 0 & 0 \\ Q_{12}^k & Q_{22}^k & 0 & 0 & 0 \\ 0 & 0 & \kappa C_{44}^k & 0 & 0 \\ 0 & 0 & 0 & \kappa C_{55}^k & 0 \\ 0 & 0 & 0 & 0 & Q_{66}^k \end{bmatrix} \quad (3)$$

or in compact form

$$\boldsymbol{\sigma}'^k = \bar{\mathbf{D}}^k \boldsymbol{\epsilon}'^k, \quad (4)$$

where  $k$  is the shear correction factor,  $\boldsymbol{\sigma}'$  and  $\boldsymbol{\epsilon}'$  are the stress and strain vectors in the material coordinate system aligned with the fiber direction. The relationship between stress and strain written with reference to the global coordinate system  $(x, y, z)$  is

$$\boldsymbol{\sigma}^k = \mathbf{D}^k \boldsymbol{\epsilon}^k \quad (5)$$

where:

$$\mathbf{D}^k = \mathbf{T}^k \bar{\mathbf{D}}^k \mathbf{T}^{k-1} \quad (6)$$

and  $\mathbf{T}^k$  is the rotation matrix [23].

The stiffness matrix is written as

$$\mathbf{K}^{(e)} = \int_V \mathbf{B}^T \mathbf{D} \mathbf{B} \, dx \, dy \, dz, \quad (7)$$

where the strain-displacement matrix is

$$\mathbf{B} = \begin{bmatrix} \varphi_{,x}^i & 0 & 0 \\ 0 & \varphi_{,y}^i & 0 \\ 0 & \varphi_{,z}^i & \varphi_{,y}^i \\ \varphi_{,z}^i & 0 & \varphi_{,x}^i \\ \varphi_{,y}^i & \varphi_{,x}^i & 0 \end{bmatrix}. \quad (8)$$

The derivatives of the displacements with respect to the global axes are obtained in the standard way using the isoparametric formulation. The numerical integration is performed by Gaussian quadrature [25]. A two-point rule suffices in the  $z$  direction, while a minimum of three or four points are needed in the  $x$  and  $y$  directions for quadratic or cubic element, respectively. Full integration is used in the  $x$  and  $y$  directions for all the terms, including the shear related terms. Otherwise, the penalty formulation of the unilateral contact may excite spurious modes (as shown in the numerical results). The integration of the element stiffness matrix is performed as a standard 18-node element with three DOF per node  $(u, v, w)$  but with the appropriate shape functions  $\varphi^i$  described previously.

The constitutive equations (4) are used to obtain the components of stress at the Gauss points. The distribution of in-plane stresses  $\sigma_x$ ,  $\sigma_{xy}$ , and  $\sigma_y$  is linear through the thickness, while the distribution of interlaminar stresses  $\sigma_{xz}$  and  $\sigma_{yz}$  obtained from constitutive equations is layer-wise constant. The new 3D plate element (3DLCS) reduces to FSDT when only one element is used through the thickness of the laminate. The 3DLCS element gives a very good representation of all the stress components except  $\sigma_z$  without the aspect ratio limitations of conventional 3D continuum elements.

### 3. CONTACT-FRICTION CONSTITUTIVE LAW

Let us consider two limited plane surfaces at a constant distance  $g$  from each other. At each point  $P$  (see Fig. 3) of the surface (a) is associated a unique point  $Q$  of the surface (b), obtained as orthogonal projection of  $P$  on (b). The kinematics of the interface is defined by the relative displacement of the two surfaces

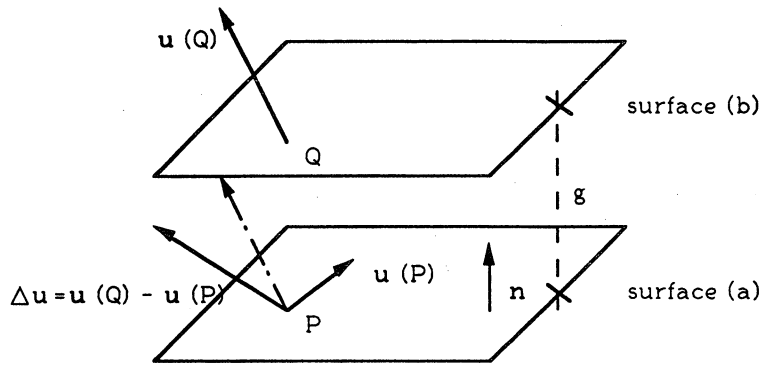


Fig. 3. Kinematics of the interface.

$$\Delta u(PQ) = u(Q) - u(P). \quad (9)$$

Denoting by  $n$  the normal to the surface (a), the relative displacement is decomposed in its normal component  $\Delta u_n = \Delta u \cdot n$  and tangential component  $\Delta v = \Delta u - \Delta u_n n$ . Let  $p$  be the contact stress vector at the interface, with normal and tangential components  $p_n$  and  $t$ , respectively. Introducing the normal penetration  $b = \Delta u_n + g$ , the normal unilateral contact constitutive equations are

$$\begin{aligned} p_n &= k_1 \Delta u_n, & \text{if } b > 0 \\ p_n &= (k_2 - k_1)g + k_2 \Delta u_n, & \text{if } b \leq 0, \end{aligned} \quad (10)$$

where  $k_1$  and  $k_2$  are constants representing the stiffnesses in the normal direction at the interface (Fig. 4).

Orthotropic friction is governed by two friction coefficients  $\mu_1$  and  $\mu_2$  relative to two orthogonal direction  $x_1$  and  $x_2$ , respectively. Obviously, when there is no contact of the surfaces, no tangential forces can be developed, then the limit tangential stress is

$$\hat{t} = 0, \quad \text{if } b > 0. \quad (11)$$

When the surfaces are in contact, a multi-linear constitutive relation, with low or high value of the

stiffness constant,  $k_4$  and  $k_3$ , according to the possibility or not of sliding, is proposed. Furthermore, the set of tangential stresses for which no slip occurs is supposed to be an ellipse with principal direction  $x_1$  and  $x_2$ . When the limit tangential stress is reached, sliding occurs in the same direction of the tangential stress.

The limit tangential stress  $\hat{t}$ , for which there is no sliding according to the Coulomb friction model, it is given by:

$$\|\hat{t}\| = -\mu p_n \quad (12)$$

with  $\mu$  friction coefficient in the direction of  $\hat{t}$ . Taking into account the proposed normal constitutive equation (10) and the definition of  $b$ , eqn (12) reduces to:

$$\|\hat{t}\| = -\mu(k_2 b - k_1 g). \quad (13)$$

The limit relative tangential displacement corresponding to the value of  $\|\hat{t}\|$  is then

$$\|\Delta \hat{v}\| = \|\hat{t}\|/k_3 = -\mu \omega \quad (14)$$

with  $\omega = (k_2 b - k_1 g)/k_3$ .

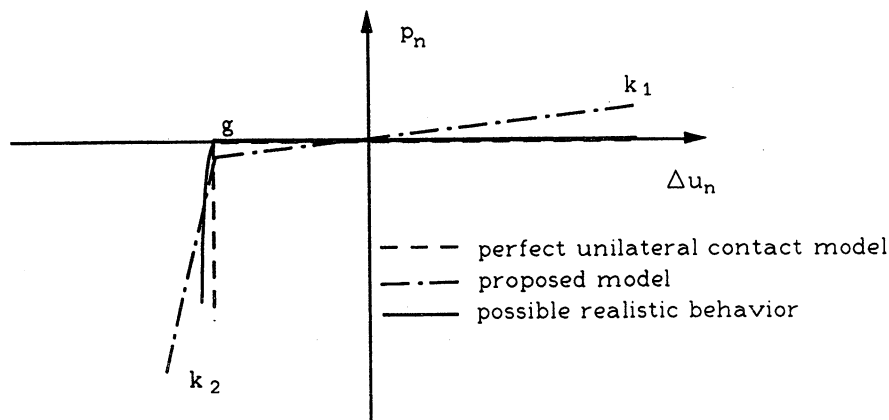


Fig. 4. Constitutive law for unilateral contact.

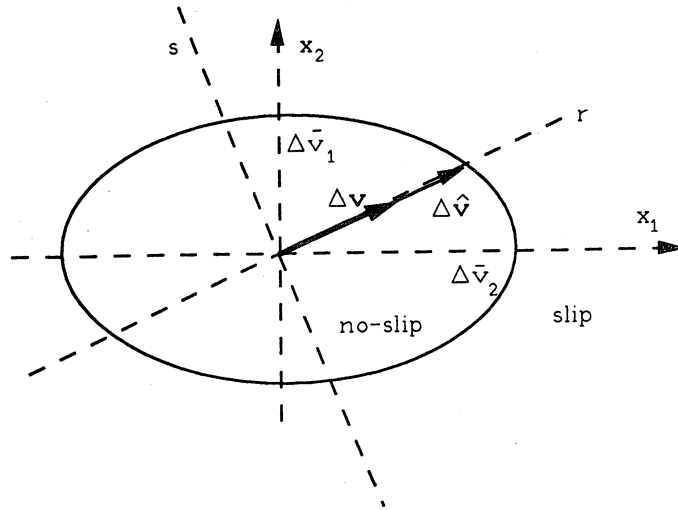


Fig. 5. Admissible set of no-slip displacement region.

The limit principal tangential relative displacements along the principal direction  $x_1$  and  $x_2$  for which there is no sliding are given by

$$|\Delta\bar{v}_1| = -\mu_1\omega, \quad |\Delta\bar{v}_2| = -\mu_2\omega. \quad (15)$$

Let us denote by  $\Delta\mathbf{v}$  and  $\Delta\hat{\mathbf{v}}$  the total and the limit tangential relative displacement in direction  $r$  (Fig. 5), respectively. Let us introduce the multiplier  $\beta$  as

$$\beta\Delta\mathbf{v} = \Delta\hat{\mathbf{v}} \quad (16)$$

and let us write the equation of the ellipse that defines the limit displacement before sliding as

$$(\Delta\hat{v}_1/\Delta\bar{v}_1)^2 + (\Delta\hat{v}_2/\Delta\bar{v}_2)^2 = 1. \quad (17)$$

Then, by taking into account eqns (15–17) we obtain

$$\beta^2 = \omega^2 / [(\Delta v_1/\mu_1)^2 + (\Delta v_2/\mu_2)^2]. \quad (18)$$

If  $\beta \geq 1$  the slip does not occur, if  $\beta < 1$  the slip does occur. It is worth noting that  $\beta$  and, moreover,  $\Delta\hat{\mathbf{v}}$  depend upon  $\Delta\mathbf{v}$ ,  $\mu_1$ ,  $\mu_2$  and upon the normal penetration  $b$ .

Equation (16) shows that when there is sliding, it occurs along the direction of  $\Delta\hat{\mathbf{v}}$  and  $\hat{\mathbf{t}}$ . This can be seen as a nonstandard flow rule, in the plane of contact, while a standard flow rule would indicate slip along the normal to the limit surface (Fig. 5).

When the slip is not possible, the constitutive equation is:

$$\mathbf{t} = k_3\Delta\mathbf{v}, \quad \text{if } b \leq 0 \text{ and } \beta \geq 1. \quad (19)$$

On the contrary, when the slip occurs, the constitutive equations in the local Cartesian co-

ordinate system  $r-s$ , with  $r$  orthogonal to  $s$ , are assumed to be

$$t_r = k_4\Delta v_r + \frac{(k_4 - k_3)\omega\Delta v_r}{\sqrt{\left(\frac{\Delta v_1}{\mu_1}\right)^2 + \left(\frac{\Delta v_2}{\mu_2}\right)^2}}$$

$$t_s = k_3\Delta v_s, \quad \text{if } b \leq 0 \text{ and } \beta < 1. \quad (20)$$

Figure 6 depicts in schematic way this constitutive relation. It can be pointed out that in the first equation of (20)  $\omega \leq 0$ . The term  $\Delta v_r / [(\Delta v_1/\mu_1)^2 + (\Delta v_2/\mu_2)^2]^{(1/2)} \geq 0$  represents the friction coefficient in  $r$  direction. The second of equations (20) constrains the slippage in the  $s$ -direction.

The constitutive equations (20) can be rewritten in the  $x_1-x_2$  coordinate system by using the rotation matrix  $\mathbf{R}$ , defined as

$$R_{11} = R_{22} = c_1, \quad R_{21} = -R_{12} = c_2 \quad (21)$$

with  $c_1 = \Delta v_1 / \|\Delta\mathbf{v}\|$  and  $c_2 = \Delta v_2 / \|\Delta\mathbf{v}\|$ . The transformation performed by  $\mathbf{R}$  is:

$$\begin{Bmatrix} \Delta v_1 \\ \Delta v_2 \end{Bmatrix} = \mathbf{R} \begin{Bmatrix} \Delta v_r \\ \Delta v_s \end{Bmatrix}, \quad \begin{Bmatrix} t_1 \\ t_2 \end{Bmatrix} = \mathbf{R} \begin{Bmatrix} t_r \\ t_s \end{Bmatrix}. \quad (22)$$

In the principal coordinate system, the tangential constitutive equation (20) is

$$\begin{Bmatrix} t_1 \\ t_2 \end{Bmatrix} = \mathbf{R} \begin{bmatrix} k_4 & 0 \\ 0 & k_3 \end{bmatrix} \mathbf{R}^T \begin{Bmatrix} \Delta v_1 \\ \Delta v_2 \end{Bmatrix} + \frac{(k_4 - k_3)\omega\|\Delta\mathbf{v}\|}{\sqrt{\left(\frac{\Delta v_1}{\mu_1}\right)^2 + \left(\frac{\Delta v_2}{\mu_2}\right)^2}} \mathbf{R} \begin{Bmatrix} 1 \\ 0 \end{Bmatrix} \quad (23)$$

if  $b \geq 0$  and  $\beta > 1$ .

Finally, the complete constitutive relations can be written in matrix form as

$$\mathbf{p} = \mathbf{K}(\Delta\mathbf{u})\Delta\mathbf{u} + \mathbf{h}(\Delta\mathbf{u})\omega + \mathbf{i}(\Delta\mathbf{u})g \quad (24)$$

with

$$\mathbf{K} = \begin{bmatrix} \alpha_1 & \alpha_{12} & 0 \\ \alpha_{12} & \alpha_2 & 0 \\ 0 & 0 & \alpha_3 \end{bmatrix}$$

$$\Delta\mathbf{v} = \begin{Bmatrix} \Delta v_1 \\ \Delta v_2 \\ \Delta u_n \end{Bmatrix}$$

$$\mathbf{h} = \begin{Bmatrix} \alpha_4 \\ \alpha_5 \\ 0 \end{Bmatrix}$$

$$\mathbf{i} = \begin{Bmatrix} 0 \\ 0 \\ \alpha_6 \end{Bmatrix} \quad (25)$$

If  $b > 0$  (no contact) then

$$\alpha_1 = \alpha_2 = \alpha_{12} = \alpha_4 = \alpha_5 = \alpha_6 = 0, \quad \alpha_3 = k_1$$

if  $b \leq 0$  (contact) then if  $\beta \geq 1$  (no slip) then

$$\alpha_1 = \alpha_2 = k_3, \quad \alpha_3 = k_2, \quad \alpha_{12} = \alpha_4 = \alpha_5 = 0,$$

$$\alpha_6 = k_2 - k_1$$

if  $\beta < 1$  (slip) then

$$\alpha_1 = k_4 c_1^2 + k_3 c_2^2, \quad \alpha_{12} = (k_4 - k_3) c_1 c_2,$$

$$\alpha_2 = k_4 c_2^2 + k_3 c_1^2$$

$$\alpha_3 = k_2, \quad \alpha_6 = k_2 - k_1$$

$$\alpha_4 = c_1(k_4 - k_3) \|\Delta\mathbf{v}\| / [(\Delta v_1/\mu_1)^2 + (\Delta v_2/\mu_2)^2]^{(1/2)}$$

$$\alpha_5 = c_2(k_4 - k_3) \|\Delta\mathbf{v}\| / [(\Delta v_1/\mu_1)^2 + (\Delta v_2/\mu_2)^2]^{(1/2)}$$

Recalling that  $\omega = (k_2 b - k_1 g)/k_3 = [k_2 \Delta u_n + (k_2 - k_1)g]/k_3$ , the constitutive equation (24) is equivalent to

$$\begin{Bmatrix} t_1 \\ t_2 \\ p_n \end{Bmatrix} = \begin{bmatrix} \alpha_1 & \alpha_{12} + \bar{\alpha}_4 & 0 \\ \alpha_{12} + \bar{\alpha}_5 & \alpha_2 & 0 \\ 0 & 0 & \alpha_3 \end{bmatrix} \begin{Bmatrix} \Delta v_1 \\ \Delta v_2 \\ \Delta u_n \end{Bmatrix} + \begin{Bmatrix} \bar{\alpha}_4 \\ \bar{\alpha}_5 \\ \alpha_6 \end{Bmatrix} g \quad (26)$$

or, in compact notation:

$$\mathbf{p} = \bar{\mathbf{K}}(\Delta\mathbf{u})\Delta\mathbf{u} + \mathbf{m}(\Delta\mathbf{u})g, \quad (27)$$

where

$$\bar{\alpha}_4 = \alpha_4 k_2 / k_3, \quad \bar{\alpha}_5 = \alpha_5 k_2 / k_3.$$

It is worth noting that when slip occurs  $\alpha_{12}$ ,  $\bar{\alpha}_4$  and  $\bar{\alpha}_5$  are not zeros and the new constitutive matrix given in (26) and (27) is not symmetric. The unsymmetry of  $\bar{\mathbf{K}}$  precludes the existence of an energy functional governing the interface constitutive relationship. The interface material can be seen as a Cauchy elastic material, that is for a given  $\Delta\mathbf{u}$  a unique  $\mathbf{p}$  can be found, but not as a Green elastic one. This means that for a closed deformation path, energy can be lost.

In order to better understand the proposed model, let us perform a simple experiment. Let us take rigid brick resting on a rigid surface. The interface between the block and the plane is modeled by the above proposed constitutive law. Let us then apply a normal force  $-F$  on the block. Vertical displacement  $\Delta u_n = -F/k_2$  occurs. Then a tangential force  $T$  is applied. Since  $F$  is fixed, the tangential limit stress is given. If  $T$  is greater than this limit tangential stress,

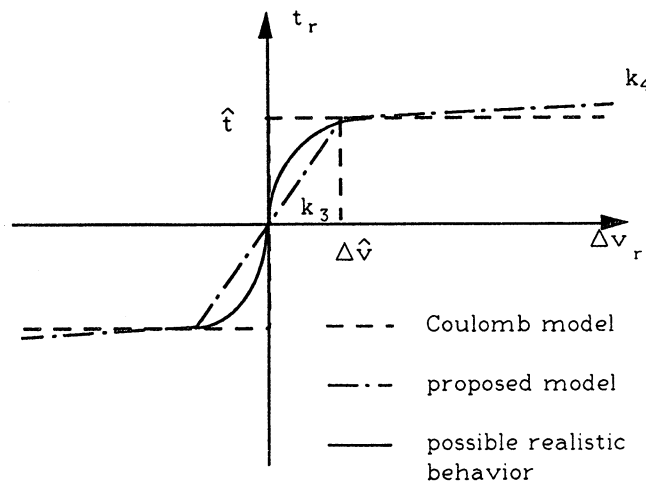


Fig. 6. Constitutive law for slip problem.

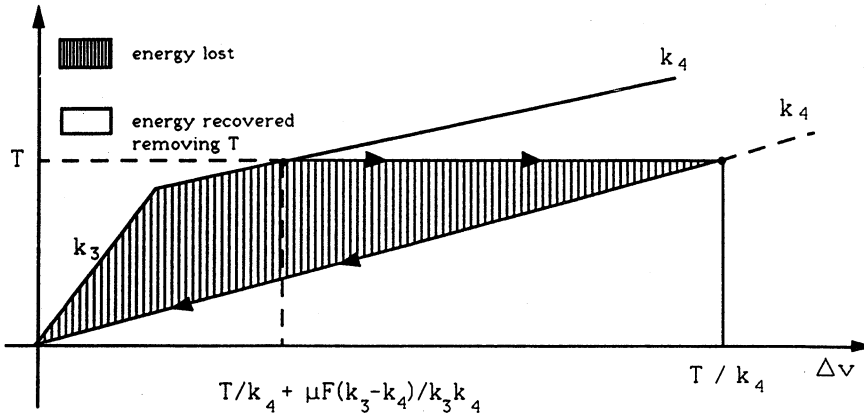


Fig. 7. Model behavior for a closed displacement path.

the horizontal displacement of the block is  $\Delta v = T/k_4 + \mu F(k_3 - k_4)/(k_3 k_4)$ . Once this condition is reached, let us remove the force  $F$ . The vertical displacement goes to zero, while the horizontal one increases to the value  $T/k_4$  in order to satisfy the equilibrium equation. The energy related to the vertical effects is recovered completely, while the one associated to the horizontal displacement increases. Removing, now, the tangential force  $T$  only some part of the spent energy is recovered as it is illustrated in Fig. 7. It seems necessary to point out that the lost energy is not transformed in heat or noise or microplasticizations of the interfaces during the slip, as occurs in the real phenomena. The model, in fact, does not consider inelastic strain. Thus it can be used efficiently only for quasi static analysis of structures subjected to a monotone increasing stress path.

4. THE INTERFACE FINITE ELEMENT

A general isoparametric 3D 18-node interface element is presented in the following. This element is developed to be used with the new 3D plate element described previously. The thickness of the element is the gap distance  $g$ , and it can be taken to be zero when surfaces are initially in contact. A schematic geometry of the element is given in Fig. 8.

The finite element formulation is carried out by starting from the variational formulation of the equilibrium equation. Since no strain energy functional can be postulated, no potential energy approach is possible, in contrast to the proposition of Beer [22]. The weak form of the governing equation can be obtained by using the virtual displacement theorem as pointed out by Schäfer [21]. The external virtual work is performed by the forces  $\mathbf{q}^{(b)}$  and  $\mathbf{q}^{(t)}$  acting on the bottom and top surfaces  $\Omega$ , times the virtual displacement  $\delta \mathbf{u}^{(b)}$  and  $\delta \mathbf{u}^{(t)}$

$$W_e = \int_{\Omega} \{ \mathbf{q}^{(b)} \cdot \delta \mathbf{u}^{(b)} + \mathbf{q}^{(t)} \cdot \delta \mathbf{u}^{(t)} \} dx_1 dx_2. \quad (28)$$

The equilibrium condition for the external forces asserts that the external work must be zero for any virtual rigid displacement ( $\delta \mathbf{u}^{(b)} = \delta \mathbf{u}^{(t)} = \delta \mathbf{u}$ )

$$W_e = \int_{\Omega} \{ \mathbf{q}^{(b)} + \mathbf{q}^{(t)} \} \cdot \delta \mathbf{u} dx_1 dx_2 = 0 \quad (29)$$

that is  $\mathbf{q}^{(b)} = -\mathbf{q}^{(t)} = \mathbf{q}$ . Thus, the external virtual work can be written correctly as

$$W_e = \int_{\Omega} \mathbf{q} \cdot \delta \Delta \mathbf{u} dx_1 dx_2. \quad (30)$$

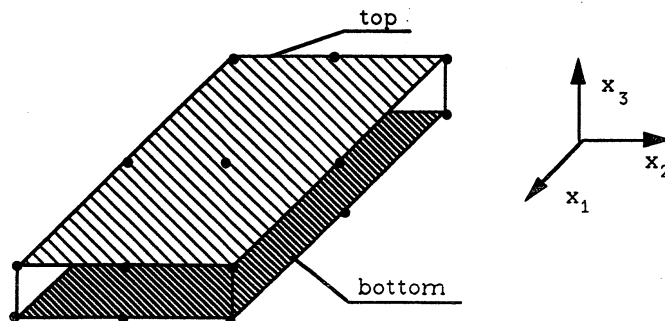


Fig. 8. Interface element.

The internal virtual work is given, using the formula (24), by

$$W_i = \int_{\Omega} \{(\mathbf{K}(\Delta\mathbf{u})\Delta\mathbf{u} + \mathbf{h}(\Delta\mathbf{u})\omega + \mathbf{i}(\Delta\mathbf{u})\mathbf{g}) \cdot \delta\Delta\mathbf{u}\} dx_1 dx_2. \quad (31)$$

Finally, the virtual displacement theorem asserts

$$\int_{\Omega} \mathbf{q} \cdot \delta\Delta\mathbf{u} dx_1 dx_2 = \int_{\Omega} \{(\mathbf{K}(\Delta\mathbf{u})\Delta\mathbf{u} + \mathbf{h}(\Delta\mathbf{u})\omega + \mathbf{i}(\Delta\mathbf{u})\mathbf{g}) \cdot \delta\Delta\mathbf{u}\} dx_1 dx_2. \quad (32)$$

According to the finite element method, the relative displacements are assumed to be

$$\begin{aligned} \Delta v_1 &= (u_1^{i+9} - u_1^i)\varphi_i \\ \Delta v_2 &= (u_2^{i+9} - u_2^i)\varphi^i \\ \Delta u_n &= (u_3^{i+9} - u_3^i)\varphi^i, \end{aligned} \quad (33)$$

where  $u_h^i$  and  $u_h^{i+9}$ , with  $h = 1, 2, 3$  and  $i = 1, 2, \dots, 9$ , are the nodal displacement of the bottom and the top of the element, respectively, in the three directions. The Lagrangian interpolation functions used are  $\varphi^i = \varphi^{i+9}$  with  $i = 1, 2, \dots, 9$ .

Substituting eqns (33) into the equilibrium equation (32) and taking into account the definition of  $\omega$ , we get

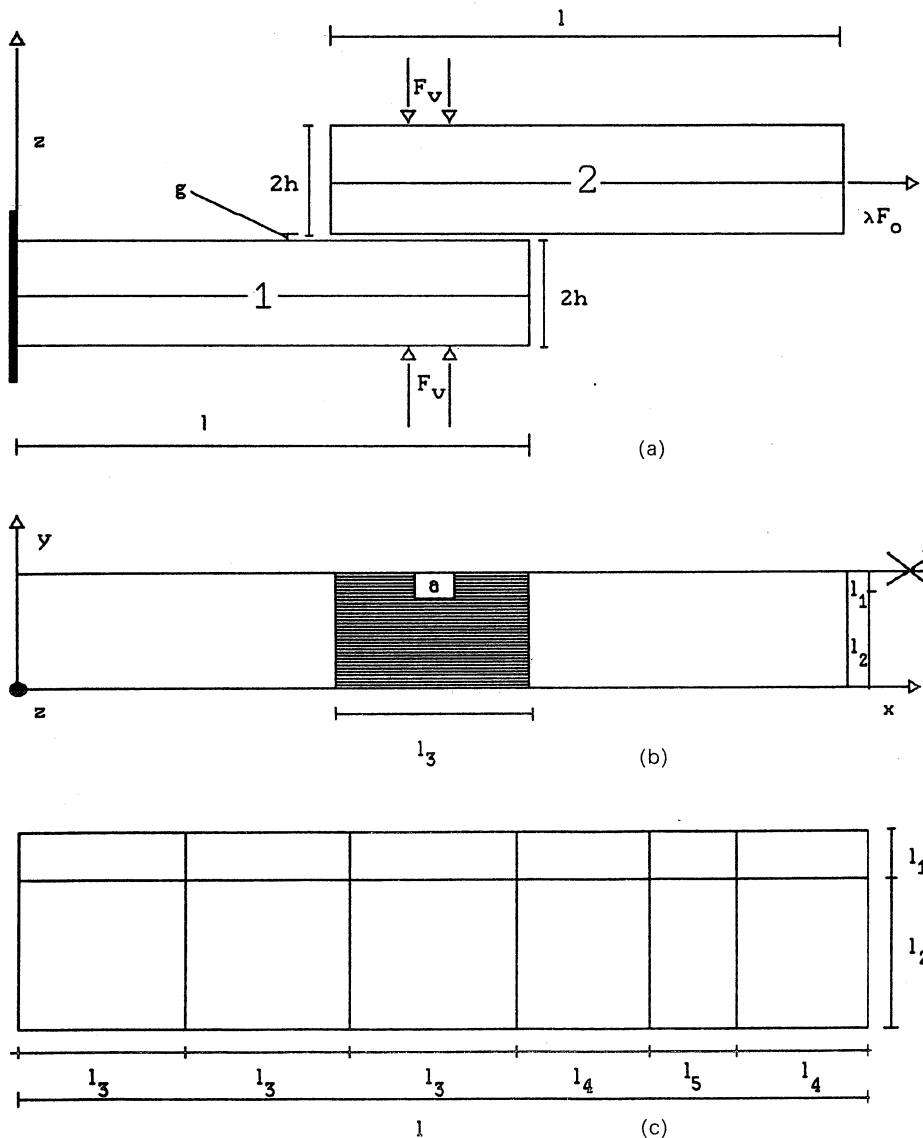


Fig. 9. Geometry of a simple model for a single lap joint and discretization of one of the two components of the joint.

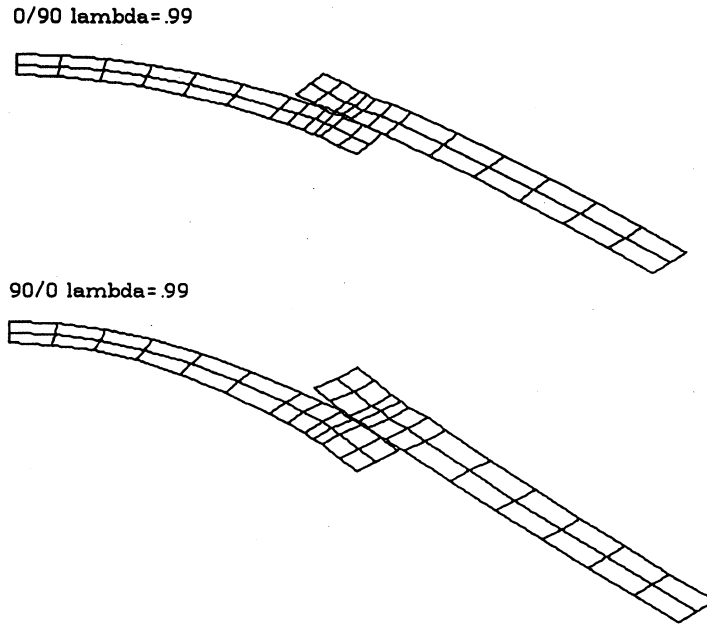


Fig. 10. Deformed shape of the joint for (0/90) and (90/0) stacking sequence for  $\lambda = 0.99$ .

$$\begin{aligned}
 \int_{\Omega} \{q_h(\delta u_h^{i+9} \varphi^{i+9} - \delta u_h^i \varphi^i)\} dx_1 dx_2 = & \int_{\Omega} \{ (K_{hk} \varphi^{i+9} - \varphi^{i+9} \varphi^i u_k^i \delta u_h^{i+9} + \varphi^i \varphi^i u_k^i \delta u_h^i) \delta_{3k} \\
 & + g \left( \frac{k_2 - k_1}{k_3} h_h + i_h \right) (\varphi^{i+9} \delta u_h^{i+9} \\
 & \times \varphi^{i+9} u_k^{i+9} \delta u_h^{i+9} - K_{hk} \varphi^i \varphi^{i+9} u_h^{i+9} \delta u_h^i \\
 & - \varphi^i \delta u_h^i) \} dx_1 dx_2 \tag{34} \\
 & - K_{hk} \varphi^{i+9} \varphi^i u_k^i \delta u_h^{i+9} + K_{hk} \varphi^i \varphi^{i+9} u_k^i \delta u_h^i) \\
 & + \frac{k_2}{k_3} h_h (\varphi^{i+9} \varphi^{i+9} u_k^{i+9} \delta u_h^{i+9} - \varphi^i \varphi^i u_k^i \delta u_h^i)
 \end{aligned}$$

with  $\delta_{3k}$  the Kronecher symbol. It is implicit that all the quantities in the eqn (34) depend of  $\Delta u$ .  
 Then, setting  $K = (j - 1) \times 3 + k$  and  $H = (i - 1) \times 3 + h$ , and reordering matrices and vectors we have

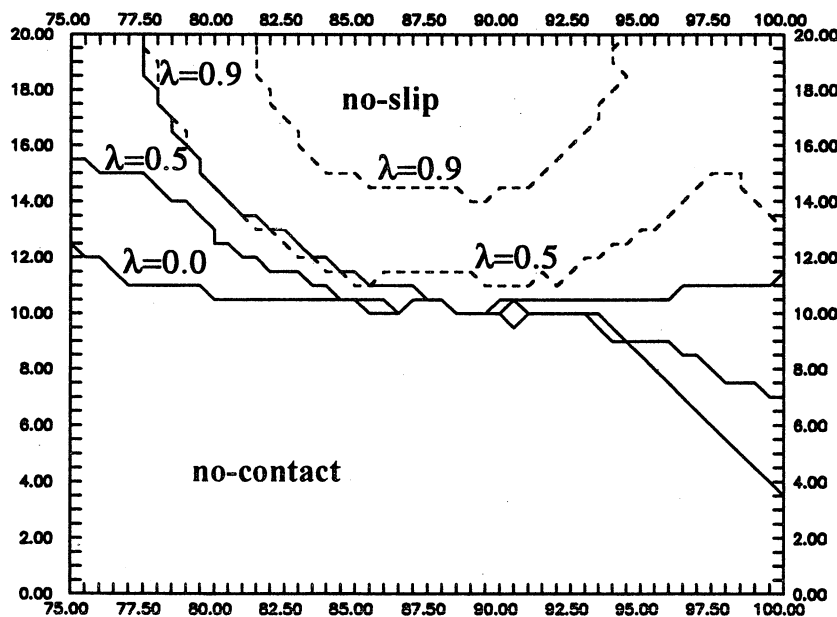


Fig. 11. Solid lines delimit the contact area with the value of the load inside the corresponding area. Broken lines delimit the no-slip area with the value of the load inside the corresponding area.

$$U_K^{(e)} = u_k^i$$

$$Q_H^{(e)} = \int_{\Omega} q_h \varphi^i dx_1 dx_2$$

$$S_{HK}^{(e)} = \int_{\Omega} K_{hk} \varphi^i \varphi^j dx_1 dx_2$$

$$H_{HK}^{(e)} = \int_{\Omega} \frac{k_2}{k_3} h_h \delta_{3k} \varphi^i \varphi^j dx_1 dx_2$$

$$I_H^{(e)} = \int_{\Omega} g \left( \frac{k_2 - k_1}{k_3} h_h + i_h \right) \varphi^i dx_1 dx_2,$$

where  $U_K^{(e)}$  is the nodal displacement vector,  $Q_H^{(e)}$  is the nodal force vector,  $S_{HK}^{(e)}$  is the secant symmetric part of the secant stiffness matrix,  $H_{HK}^{(e)}$  is the secant unsymmetric part of the secant stiffness matrix,  $I_H^{(e)}$  is secant gap vector and the superscript  $(e)$  indicates an elemental quantity.

The numerical integration scheme used is very important for the correct determination of the matrices and vectors involved in the interface finite element. In fact, Gauss quadrature can provide exact integration as long as the element is fully in contact

of fully separated and simultaneously is in complete no-slipping or complete slipping. Obviously, unless a very fine mesh is adopted, these cases are very rare. For an element in partial contact and slip, the constitutive equations are very different for the contact and separated portions of the element. Therefore, the Gauss integration rule does not give a satisfactory approximation of the quantities defining the interface element. In order to overcome this difficulty, the simple and effective Simpson numerical integration is used, with a large number of Simpson integration points. This integration technique requires some CPU time for the evaluation of the interface element matrices and vectors. However, a large number of integration points produces a good evaluation of the contribution to the nodes of the stiffness of the unilateral and friction element by representing correctly the contact, no-contact, slip, and no-slip areas. The refined integration scheme proposed is an inexpensive substitute for mesh refinement, which would be necessary if nodal contact/friction springs were used, or if the proposed element were to be integrated with a three-point Gauss quadrature.

Finally, the equilibrium equation can be written in matrix form as:

$$Q^{(e)} = S^{(e)}(U^{(e)})U^{(e)} + H^{(e)}(U^{(e)})U^{(e)} + I^{(e)}(U^{(e)}). \tag{35}$$

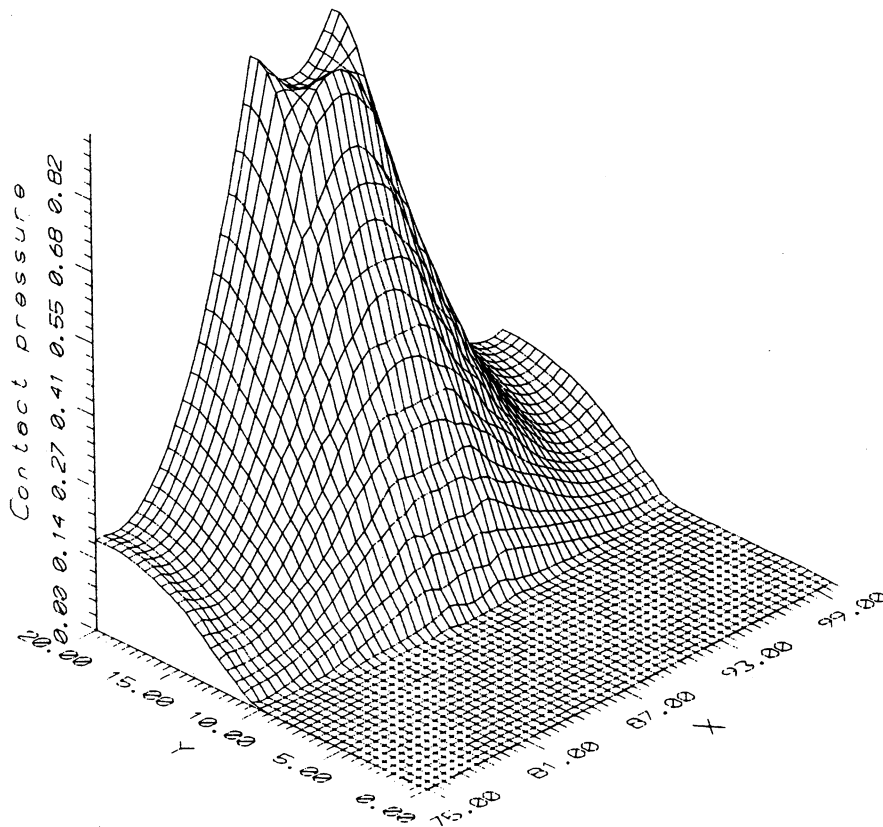


Fig. 12. Contact pressure between (0/0) plates for  $\lambda = 0.0$ .

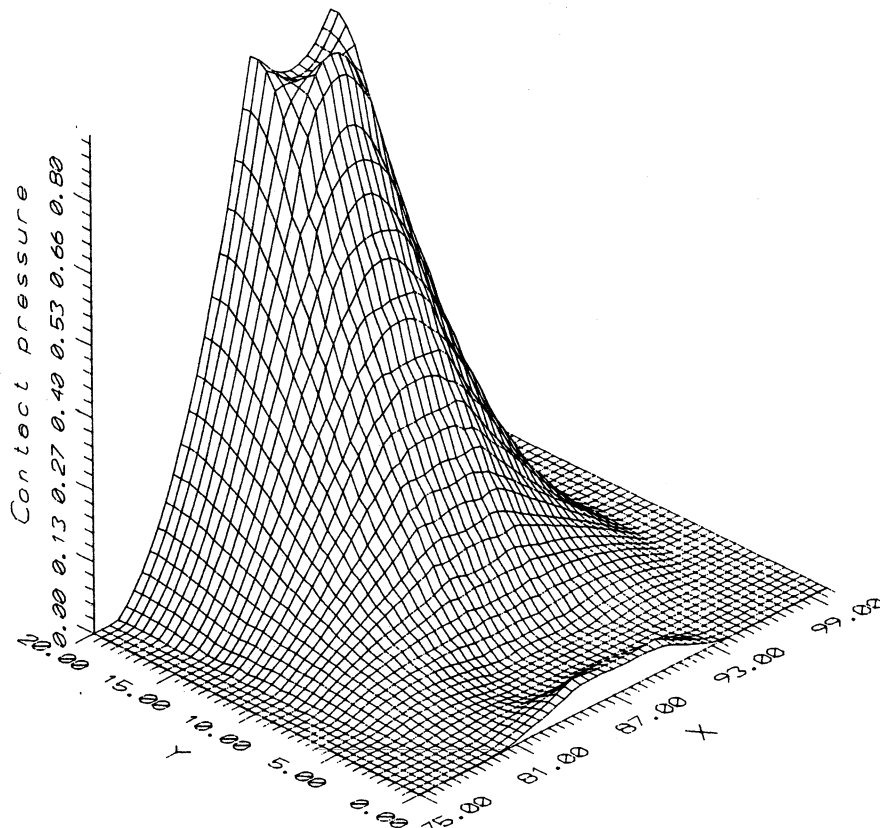


Fig. 13. Contact pressure between (90/90) plates for  $\lambda = 0.0$ .

### 5. NUMERICAL PROCEDURE

Once the stiffness matrix of the 3D plate element and the discrete governing equation for the 3D interface element are defined, by assembling all the interface and plate elements of the discretization, the following nonlinear algebraic system of equations is obtained:

$$\mathbf{S}(\mathbf{U})\mathbf{U} = \mathbf{Q} - \mathbf{H}(\mathbf{U})\mathbf{U} - \mathbf{I}(\mathbf{U}), \quad (36)$$

where  $\mathbf{S}(\mathbf{U})$  is the symmetric matrix of the stiffness of the whole structure obtained by assembling the symmetric stiffness matrices of the plate elements and the symmetric part of the secant stiffness interface element,  $\mathbf{Q}$  is the global nodal force vector,  $\mathbf{H}(\mathbf{U})$  is the unsymmetric part of the secant stiffness matrix,  $\mathbf{I}(\mathbf{U})$  is gap vector.

The nonlinear problem (36) is approached by using an iterative procedure based on the direct iteration method. The solution at  $i$ th step is given in terms of that obtained at previous one by the formula

$$\mathbf{U}^i = [\mathbf{S}(\mathbf{U}^{i-1})]^{-1} \{ \mathbf{Q} - \mathbf{H}(\mathbf{U}^{i-1})\mathbf{U}^{i-1} - \mathbf{I}(\mathbf{U}^{i-1}) \}. \quad (37)$$

The force vector  $\{ \mathbf{Q} - \mathbf{H}(\mathbf{U}^{i-1})\mathbf{U}^{i-1} - \mathbf{I}(\mathbf{U}^{i-1}) \}$  is constructed at element level. The matrix  $\mathbf{H}(\mathbf{U}^{i-1})$  and

the vector  $\mathbf{I}(\mathbf{U}^{i-1})$  are not assembled at the global level.

The convergence is reached when the error  $\text{Err} = \|\mathbf{U}^i - \mathbf{U}^{i-1}\| / \|\mathbf{U}^i\| \leq \gamma$ , with  $\gamma$  assigned admissible error. This kind of test may induce error in the evaluation of the approximate solution. In fact, during the iterations it may occur that although the value of Err is very small we are far from the solution. This happens because the displacements of the nodes during two successive iterations are very close almost everywhere except in only few nodes in the contact region. Then, we propose a convergence test based on a new definition of  $\text{Err} = \|U_p^i - U_p^{i-1}\| / \|U_p^i\|$ , where  $p$  is a set of points at which the response is very sensitive to the contact and slip problem. The described iterative procedure is not based, like many procedures proposed in specialized literature, on the numerical decoupling of two problems: the contact and the friction [25]. On the contrary, the numerical procedure proposed here treats the coupled problem.

The contact/friction element has three DOF per node on all the nodes. The 3D plate element has two DOF per node on all the nodes except in the master nodes of the laminate, shown as solid squares in Fig. 2. Each of the plates in contact has a set of master nodes, but they are not necessarily located in a position adjacent to the contact/friction elements. Since the position of the master nodes through the thickness of the plate is irrelevant, the case of two

plates in contact could be modeled by setting the master nodes at the surfaces in contact. To model a more general case (e.g., double lap connection) it is required that contact/friction elements be connected to nodes on both surfaces of the plate. This has been accomplished by implementing the capability to identify nodes associated to interface elements, then assigning the  $w$ -contribution of the interface element to the stiffness of the master nodes.

## 6. NUMERICAL RESULTS

A simple problem is studied in the following to show the capability of the 3D plate element, the 3D interface element and the numerical procedure developed. Let us consider a bolted single lap joint with two identical components as shown in Fig. 9. Each plate is composed by two layers with a thickness  $h$  and each layer is characterized by an orientation of the fibers  $\vartheta_i$  (angle between the direction of the fibers and the  $x$  axis). The dimensions of the plates are  $l = 20h$ ,  $l_1 = h$ ,  $l_2 = 3h$ ,  $l_3 = 5h$  and  $g = 0.0$ . Plate 1 is constrained along the side  $x = 0$  and the contact surface between the two plates is represented by the shaded area in Fig. 9(b).

Two friction coefficients  $\mu_1 = \mu_2 = 0.5$  characterize the contact surface, and the elastic moduli of each plate are:  $E_1/E_2 = 40$ ,  $\nu_{12} = \nu_{23} = 0.25$ ,  $G_{12}/E_2 = 0.5$ , where subscripts 1, 2 and 3 indicate the direction of

the fiber, perpendicular to them, and perpendicular to the plate, respectively. A vertical load  $F_v$  distributed along the perimeter of the rectangle  $a$  is applied and an horizontal distributed force  $\lambda F_0$  is applied on the plate 2 as shown in Fig. 9(a). The following values of the forces are used:  $F_v/E_2 h^2 = 7 \times 10^{-5}$  and  $F_0 = \mu F_v$ .

Because of the symmetry of the structure, only one half of the structure is modeled in the finite element analysis with 24 elastic elements for each plate and six interface elements for the contact surface. The interface elements are integrated using 100 Simpson equally spaced points in each direction. The mesh used for of each layer in the plane  $x-y$  is shown in Fig. 9(c) where  $l_4 = 2h$  and  $l_5 = h$ .

The following set of regularization parameters (see Figs 4 and 6) is adopted in the computations:  $k_1 2h/E_2 = 10^{-6}$ ,  $k_2 2h/E_2 = 1$ ,  $k_3 = k_2$  and  $k_4 = k_1$ . There are several constraints for the selection of the value of the contact stiffness  $k_2$ . The value of  $k_2$  is limited by the ability of the mesh size to capture the wavelength of the unilateral contact solution. Another limit is set by the difficulty in achieving convergence of the numerical solution as the value of  $k_2$  increases, because of the ill-conditioning of the secant stiffness matrix at each iteration. Finally, the contact stiffness should allow for a certain degree of transverse deformability of the two plates, which is absent in the incompressible plate elements.

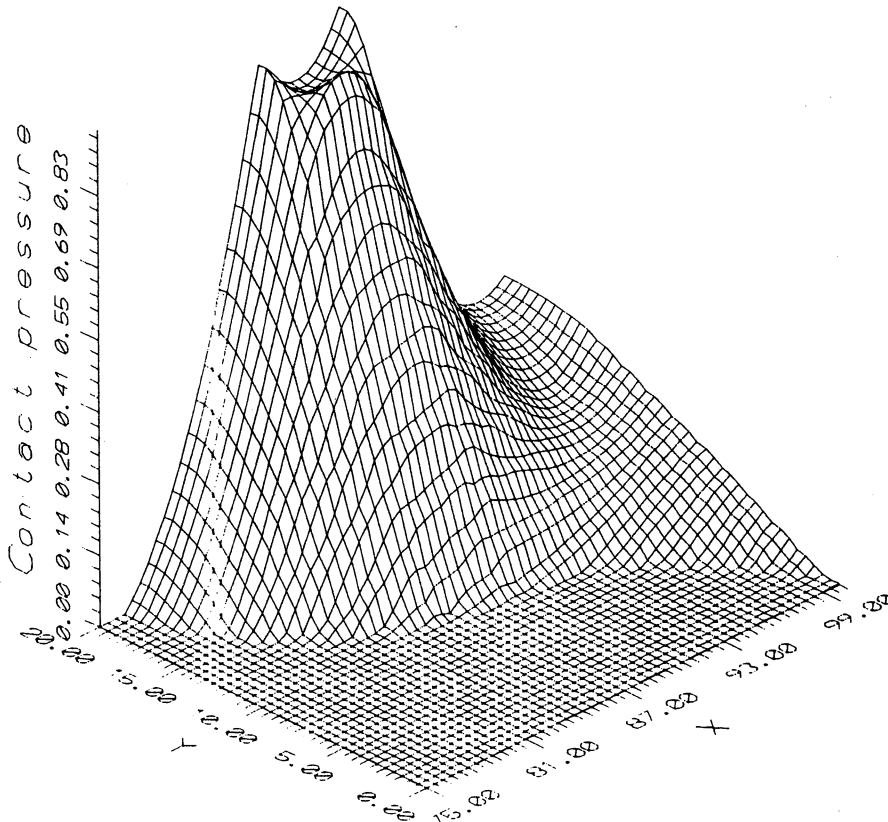


Fig. 14. Contact pressure distribution for joint with (0/0) stacking sequence, for  $\lambda = 0.9$ .

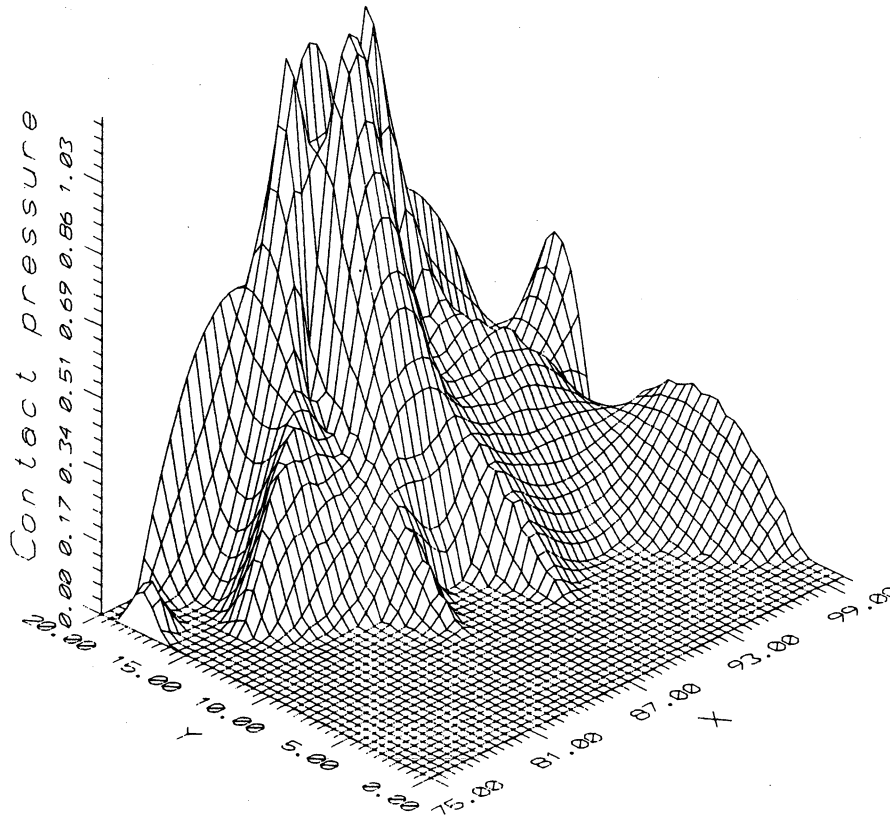


Fig. 15. Contact pressure distribution for joint with (0/0) stacking sequence, for  $\lambda = 0.9$ , using reduced integration for shear terms in the plate elements.

Four cases are considered, each characterized by the orientation of the fibers in the two layers of each plate. The first case has  $\vartheta_1 = 0^\circ$  and  $\vartheta_2 = 0^\circ$ , the second case  $\vartheta_1 = 0^\circ$  and  $\vartheta_2 = 90^\circ$ , the third case  $\vartheta_1 = 90^\circ$  and  $\vartheta_2 = 0^\circ$  and the fourth case  $\vartheta_1 = 90^\circ$  and  $\vartheta_2 = 90^\circ$ . For the (0/90) and (90/0) case, the deformation of the structure for a load parameter  $\lambda = 0.99$  is presented in Fig. 10 with the displacements magnified 3000 times. In the second (0/90) and third (90/0) case, for the same value of the eccentric horizontal force  $\lambda F_0$ , the curvature and the displacements of the structure are different, because of the different bending-extension coupling stiffness of the plates.

For the case (0/0) the contact zone for  $\lambda = 0.0, 0.5$  and  $0.9$  and the slip zone for  $\lambda = 0.5$  and  $0.9$  are shown in Fig. 11. Solid lines delimit the contact area with the value of the load multiplier  $\lambda$  inside the corresponding area. Broken lines delimit the no-slip area with the value of the multiplier load  $\lambda$  inside the corresponding area. The distribution of the contact zone changes by increasing the parameter  $\lambda$ . The contact zone moves because of the inflection of the plates caused by the eccentricity of the horizontal force  $\lambda F_0$ . The contact pressure distribution for the case  $\lambda = 0.0$  is shown in Fig. 12. Next, in Fig. 13 the contact pressure is plotted for the lamination (90/90) with  $\lambda = 0.0$ . It is worth noting the different shape of

the contact zone for the two cases 0/0 and 90/90 when  $\lambda = 0.0$ . In both cases the contact zone is oriented in the direction of the fibers. For all cases studied complete slip occurs exactly when  $\lambda F_0 = \mu F_r$ , that is for  $\lambda = 1$ .

The contact pressure distribution for the case (0/0) is shown in Fig. 14 for  $\lambda = 0.9$ . If reduced integration of the shear terms is used, spurious modes may be excited by the penalization of the unilateral contact problem. This may lead to lack of convergence, or if convergence can be achieved, to erroneous results. One such case is presented in Fig. 15 where the contact pressure distribution for the same case and same load condition used in Fig. 14 is shown. The erratic behavior is caused by the use of the reduced integration in combination with the unilateral penalty approach.

Since it is required to use full integration, a plate element with minimum shear locking is required. In this work, this requirement is satisfied by the 3D plate element presented by virtue of the following features. First, a nine-node Lagrangian interpolation is used. Second, the shear strain, thus the energy, is well approximated by a layer-wise constant distribution through the thickness. The accuracy of the approximation to the shear energy increases as the number of layers used to model the laminate increases. In fact even the need to use a shear correction factor  $k$  in the

plate elements reduces as the number of elements through the thickness of the laminate increases. This can be explained for the case of an homogeneous plate as follows. An assemblage of 3DLCS elements through the thickness represents the parabolic distribution of shear stress by a layer-wise constant approximation. As the number of layers increases the error reduces and no shear correction factor is needed.

## 7. CONCLUSIONS

A combination of the 3D plate element and 3D interface element is presented for the analysis of joints of laminated composite plates. A simple and effective numerical procedure is presented for the solution of the nonlinear problem. The applicability of the model is demonstrated by simple numerical examples. The numerical model presented is able to capture the salient features of the problem even using a coarse discretization. For the case of normal pressure, the contact zone is oriented along the fiber direction as a result of the higher stiffness of the plates in this direction. When a horizontal load is applied, the contact zone and the overall deflection of the plates is well represented including the effects of bending-extension coupling. Complete slip is predicted at the correct value of load according to Coulomb law. The need for using a fully integrated plate element is documented. Implementation of both the elements presented into a commercial finite element package is underway, to be able to analyze more complex geometries.

*Acknowledgements*—This work has been completed thanks to the financial support from Consiglio Nazionale delle Ricerche in Italy, the Constructed Facilities Center at West Virginia University, and NATO Grant CRG 910943.

## REFERENCES

1. J. R. Doyle, Behavior of bolt and adhesive connections in glass fiber reinforced plastic members. M.S. thesis, West Virginia University (1991).
2. J. Bortman and B. A. Szabó, Nonlinear models for fastened structural connections. *Comput. Struct.* **43**, 909–923 (1992).
3. J. N. Reddy, Exact solutions of moderately thick laminated shells. *ASCE J. Engng Mech. Div.* **110**, 794 (1984).
4. S. Srinivas, Refined analysis of composite laminates. *J. Sound Vibr.* **30**, 495–507 (1973).
5. M. Epstein and P. G. Glockner, Non-linear analysis of multilayered shells. *Int. J. Solid Struct.* **13**, 1081–1089 (1977).
6. P. Seide, An improved approximate theory for the bending of laminated plates. *Mechanics Today* **5**, 451–466 (1980).
7. M. Epstein and H. P. Huttelmaier, A finite element formulation for multilayered and thick plates. *Comput. Struct.* **16**, 645–650 (1983).
8. H. Murakami, Laminated composite plate theories with improved inplane responses. *ASME Pres. Vessel and Piping Conf.*, pp. 257–263 (1984).
9. D. R. J. Owen and Z. H. Li, A refined analysis of laminated plates by finite element displacement methods. I Fundamentals and static analysis; II Vibrations and stability. *Comput. Struct.* **26**, 907–923 (1987).
10. J. N. Reddy, A generalization of two dimensional theories of laminated plates. *Commun. Appl. Numer. Meth.* **3**, 113–180 (1987).
11. E. J. Barbero, On a generalized laminated plate theory with application to bending, vibration, and delamination buckling in composite laminates. Ph.D. dissertation, Virginia Polytechnic Institute and State University, Blacksburg, VA (1989).
12. E. J. Barbero, 3-D finite element modeling of laminated composites by layer-wise constant shear elements. NDE Vol. 10, *Enhanced Analysis Techniques for Comp. Mater.*, ASME, pp. 229–237 (1991).
13. E. J. Barbero, A 3-D finite element for laminated composites with 2-D kinematic constraints. *Comput. Struct.* **45**, 263–271 (1992).
14. S. Ahmad, B. M. Irons and O. C. Zienkiewicz, Analysis of thick and thin shell structures by curved finite elements. *Int. J. Numer. Meth. Engng* **2**, 419–451 (1970).
15. P. Panagiotopoulos, *Inequality Problems in Mechanics. Convex and Nonconvex Energy Functions*. Birkhäuser, Basel (1985).
16. N. Kikuchi and J. T. Oden, Contact problems in elasticity: a study of variational inequality and finite element method. *SIAM Studies in Applied Mathematics*, Philadelphia, PA (1988).
17. A. Villaneuva-Leal and S. Hinduja, Modelling the characteristics of interface surfaces by the finite element method. *Proc. Inst. Mech. Engrs* **198C**, 9–23 (1984).
18. A. Grimaldi, R. Luciano and E. Sacco, Unilateral and friction model for the monumental structures. Report No. 34, Civil Engineering Department, University of Rome, Tor Vergata.
19. A. Grimaldi, R. Luciano and E. Sacco, Nonlinear dynamic analysis of masonry structures via F.E.M. *Proceedings of 10th International Conference on Computing Methods in Applied Science and Engineering*, Le Vesinet (Parigi) (1992).
20. R. E. Goodman, R. L. Taylor and T. K. Brekke, A model for the mechanics of jointed rocks. *J. Soil Mech. Found. Div.*, ASCE 637–658 (1968).
21. H. Schäfer, A contribution to the solution of contact problems with the aid of bond elements. *Comput. Meth. Appl. Mech. Engng* **6**, 335–354 (1975).
22. G. Beer, An isoparametric joint/interface element for finite element analysis. *Int. J. Numer. Meth. Engng* **21**, 585–600 (1985).
23. R. M. Jones, *Mechanics of Composite Materials*. Hemisphere, New York (1975).
24. J. N. Reddy, *Energy and Variational Methods*, John Wiley, New York (1984).
25. R. D. Cook, *Concepts and Applications of Finite Element Analysis*, 2nd Edn. John Wiley, New York (1974).
26. G. E. Stavroulakis and P. D. Panagiotopoulos, Convex multilevel decomposition algorithms for non-monotone problems. *Int. J. Numer. Meth. Engng* **36**, 1945–1966 (1993).

